SIAM J. APPL. MATH.
Vol. 57, No. 3, pp. 631–648, June 1997

004

QUALITATIVE PROPERTIES OF STEADY-STATE POISSON–NERNST–PLANCK SYSTEMS: PERTURBATION AND SIMULATION STUDY*

V. BARCILON†, D.-P. CHEN‡, R. S. EISENBERG‡, AND J. W. JEROME§

Abstract. Poisson–Nernst–Planck (PNP) systems are considered in the case of vanishing permanent charge. A detailed case study, based on natural categories described by system boundary conditions and flux, is carried out via simulation and singular perturbation analysis. Our results confirm the rich structure inherent in these systems. A natural quantity, the quotient of the Debye and characteristic length scales, serves as the singular perturbation parameter. The regions of validity are carefully analyzed by critical comparisons and contrasts between the simulation and the perturbation solution, which can be represented in closed form.

Key words. Poisson–Nernst–Planck systems, simulation, singular perturbation solution, boundary layer solution, interior solution, categories of boundary conditions

AMS subject classifications. 34A34, 34A50, 34B15, 34D15, 92C05, 92C35

PII. S0036139995312149

Introduction. We shall pursue our investigation of the properties of the steady-state PNP equations, initiated in the previous paper [9]. In order to make the presentation as self-contained as possible, we very briefly recall the basic problem.

We are concerned with the distributions p and n of two species of ions, respectively, with unit positive and unit negative charges. The distribution of these ions is the result of the balance between a diffusive process and the action of an electric potential ϕ, which is itself controlled by the ion distributions. Thus, the potential is governed by the Poisson equation, viz.,

$$\lambda^2\phi'' - n + p = 0, \tag{1}$$

while the following Nernst–Planck equations govern the distributions of ions, which are assumed to have identical mobilities:

$$n' - n\phi' = J_n, \tag{2}$$

$$p' + p\phi' = -J_p. \tag{3}$$

The system (1)–(3) is generally referred to in the literature as an electrodiffusion system (cf. [10]). It has been shown to be well posed in [6]. Two remarks must be made at this stage. First, the above equations are written in dimensionless units. We refer the reader to [9] for a discussion of the nondimensionalization process. We draw attention to the dimensionless parameter λ^2, which is related to the ratio of the Debye length to a characteristic length scale. We shall say more about this parameter in

*Received by the editors November 19, 1995; accepted for publication (in revised form) February 27, 1996.

http://www.siam.org/journals/siap/57-3/31214.html

†Department of Geophysical Sciences, University of Chicago, Chicago, IL 60637 (barcilon@math.uchicago.edu).

‡Department of Molecular Biophysics and Physiology, Rush Medical College, Chicago, IL 60612 (duanpin@aix550.phys.rpslmc.edu, bob@aix550.phys.rpslmc.edu). This research was supported by National Science Foundation grant BIR-9205688.

§Department of Mathematics, Northwestern University, Evanston, IL 60208 (jwj@math.nwu.edu). This research was supported by National Science Foundation grant DMS-9123208.

what follows. Secondly, these equations are one dimensional. Strictly speaking, for the physiological applications we have in mind (cf. [5]), we would have liked to consider the same problem in tubelike channels. However, many physiological channels are long and narrow. By exploiting the smallness of the aspect ratio, we can often reduce these problems to one-dimensional ones, as was done in [1]. This is our justification for considering this case. The dimensionless spatial variable x will therefore span the interval $[0, 1]$. Derivatives with respect to x are indicated by primes.

To understand the motivation of this paper, it might be helpful to review briefly those results of [9] which will be useful here. Several of these results are related to what were called "simple boundary conditions," viz.,

$$p = n = c_L, \qquad \phi = V \quad \text{for} \quad x = 0, \tag{4}$$

$$p = n = c_R, \qquad \phi = 0 \quad \text{for} \quad x = 1. \tag{5}$$

These boundary conditions arise naturally if the ion distributions obey charge neutrality at the endpoints. Depending on the ordering of c_L and c_R, as well as the sign of V, p lies either above or below n and ϕ is either concave or convex. In all cases

$$IV \geq 0, \tag{6}$$

where

$$I = J_n + J_p \tag{7}$$

is the total ionic current. These results are valid for all values of λ. In addition, the solution is uniquely determined.

For general boundary conditions, namely,

$$p = p_L, \quad n = n_L, \qquad \phi = V \quad \text{for} \quad x = 0, \tag{8}$$

$$p = p_R, \quad n = n_R, \qquad \phi = 0 \quad \text{for} \quad x = 1; \tag{9}$$

the only rigorous results obtained dealt with the number of crossings of the p and n distributions.

Since the ion distributions are not controlled at the ends of channel but rather are determined by the processes present in the baths on either side of the membrane, these general boundary conditions are very relevant physiologically. We would like to explore the resulting profiles by other means. In this paper, we shall use both asymptotic and numerical techniques to examine these boundary conditions.

The asymptotic analysis will be confined to the case where the dimensionless parameter λ is small. In fact, to stress this restriction, we shall change our notation and write

$$\lambda^2 = \varepsilon^2 << 1. \tag{10}$$

It so happens that for the physiological cases of interest, λ is of order 10^{-2} and thus small. This is the value which we shall also use in our numerical investigations of the problem.

As is implicit in [9], we shall see that many of the results for simple boundary conditions do not hold for general ones. In particular, the curvature of ϕ is not of one sign. Also, the inequality (6) no longer holds. In other words, the sign of V does not determine the direction of the current. Fortunately, by using matched

asymptotic expansions, we shall be able to derive *complete, explicit* expressions for all the zeroth-order fields. However, the numerical calculations will show that such asymptotic expansions, even for the same value of ε, do not always have the same degree of reliability.

There are other reasons for embarking on an asymptotic analysis of the problem. It hints at certain combinations of parameters which determine the global results. In particular, we shall see that $\sqrt{n_R p_L / p_R n_L}\exp V$ and $\sqrt{p_R n_R / p_L n_L}$ determine the signs of zeroth-order fluxes. Unfortunately, this is just a hint, and there is no guarantee that such a lower-dimensional manifold exists for all values of λ.

Finally, we should mention one more reason for undertaking an asymptotic analysis. It is related to the fact that the same problem (i.e., with general boundary conditions) has already appeared in the literature [3]. Unfortunately, an error in the approach of Cohen and Cooley [3] vitiates their results. We shall review their approach and indicate where their analysis requires remediation.

1. Singular perturbation study. Consider the PNP equations, which we rewrite here as

$$\varepsilon^2 \phi'' - n + p = 0, \tag{11}$$

$$n' - n\phi' = J_n, \tag{12}$$

$$p' + p\phi' = -J_p \tag{13}$$

in $\Omega = (0,1)$ with general boundary conditions

$$p(0) = p_L > 0, \quad n(0) = n_L > 0, \tag{14}$$

$$p(1) = p_R > 0, \quad n(1) = n_R > 0, \tag{15}$$

$$\phi(0) = V, \quad \phi(1) = 0. \tag{16}$$

We think of $\lambda = \varepsilon$ as a small parameter, and we use the method of matched asymptotic expansion to derive the solutions, particularly those to be computed later in the simulations.

1.1. The interior solution. First, we look for an approximate solution in the interior of the form

$$\phi = \Phi^{(0)} + \varepsilon \Phi^{(1)} + \cdots, \tag{17}$$

$$n = N^{(0)} + \varepsilon N^{(1)} + \cdots, \tag{18}$$

$$p = P^{(0)} + \varepsilon P^{(1)} + \cdots. \tag{19}$$

From the point of view of limit process expansions, these series are obtained by holding x fixed and letting $\varepsilon \downarrow 0$. To zeroth order in ε, the problem reduces to

$$N^{(0)} - P^{(0)} = 0, \tag{20}$$

$$N^{(0)'} - N^{(0)}\Phi^{(0)'} = J_n^{(0)}, \tag{21}$$

$$P^{(0)'} + P^{(0)}\Phi^{(0)'} = -J_p^{(0)}. \tag{22}$$

Note that (20) implies that we have charge neutrality in the interior and therefore

$$P^{(0)} = N^{(0)} = C^{(0)}. \tag{23}$$

Adding and subtracting the flux formulas, we deduce that

$$J^{(0)} = 2C^{(0)'},$$
$$-I^{(0)} = 2C^{(0)}\Phi^{(0)'}.$$

Clearly,

$$C^{(0)} = \frac{J^{(0)}}{2}\left(x + a^{(0)}\right). \tag{24}$$

Thus, the concentrations are linear in x. Also,

$$\Phi^{(0)} = -\frac{I^{(0)}}{J^{(0)}}\ln(x + a^{(0)}) + b^{(0)}. \tag{25}$$

These interior solutions, which contain the four unknown constants $J^{(0)}, I^{(0)}, a^{(0)}$, and $b^{(0)}$, cannot in general satisfy all the six boundary conditions (14)–(16). Thus, different representations for the solution must be valid near the endpoints of the interval. These are the boundary layer representations, which we consider next.

1.2. The boundary layer solutions. We consider the left boundary layer, i.e., the one near $x = 0$, first. We introduce the stretched coordinate

$$x = \varepsilon\zeta$$

and express the various fields in terms of this coordinate as

$$p(\varepsilon\zeta;\varepsilon) = \varpi(\zeta;\varepsilon),$$
$$n(\varepsilon\zeta;\varepsilon) = \mu(\zeta;\varepsilon),$$
$$\phi(\varepsilon\zeta;\varepsilon) = \psi(\zeta;\varepsilon).$$

Each of these fields is written as an asymptotic series, namely,

$$\varpi(\zeta;\varepsilon) = \varpi^{(0)}(\zeta) + \varepsilon\varpi^{(1)}(\zeta) + \cdots,$$
$$\mu(\zeta;\varepsilon) = \mu^{(0)}(\zeta) + \varepsilon\mu^{(1)}(\zeta) + \cdots,$$
$$\psi(\zeta;\varepsilon) = \psi^{(0)}(\zeta) + \varepsilon\psi^{(1)}(\zeta) + \cdots.$$

These representations are obtained by holding ζ fixed and letting $\varepsilon \downarrow 0$. The problem for the leading order fields is

$$0 = \varpi^{(0)}_{\zeta} + \varpi^{(0)}\psi^{(0)}_{\zeta},$$
$$0 = \mu^{(0)}_{\zeta} - \mu^{(0)}\psi^{(0)}_{\zeta},$$
$$-\psi^{(0)}_{\zeta\zeta} = \varpi^{(0)} - \mu^{(0)}, \tag{26}$$

with

$$\varpi^{(0)}(0) = p_L,$$
$$\mu^{(0)}(0) = n_L,$$
$$\psi^{(0)}(0) = V.$$

To this formulation we must add the requirement that these boundary layer fields match the interior fields in some domain where both representations are valid (see

[8]). As a consequence of this matching, further boundary conditions are obtained, which we shall give shortly. First, we integrate the boundary layer version of the Nernst–Planck equations and write

$$\varpi^{(0)} = p_L e^{-\psi^{(0)}+V}, \tag{27}$$

$$\mu^{(0)} = n_L e^{\psi^{(0)}-V}. \tag{28}$$

Substituting these expressions for the concentrations in the Poisson equation, we see that

$$-\psi^{(0)}_{\zeta\zeta} = p_L e^{-(\psi^{(0)}-V)} - n_L e^{(\psi^{(0)}-V)}. \tag{29}$$

We can also integrate this equation once after multiplying it by $\psi^{(0)}_\zeta$:

$$-\frac{1}{2}(\psi^{(0)}_\zeta)^2 + \frac{1}{2}(c^{(0)})^2 = -p_L(e^{-(\psi^{(0)}-V)} - 1) - n_L(e^{\psi^{(0)}-V} - 1). \tag{30}$$

Further progress requires a consideration of the matching of the two representations. This is usually done by introducing an intermediate variable such as x_α, where

$$\begin{aligned} x_\alpha &= \varepsilon^{-\alpha} x, \\ x_\alpha &= \varepsilon^{1-\alpha}\zeta, \end{aligned}$$

and $0 < \alpha < 1$ and by investigating the result of the limit process $\{x_\alpha$ fixed $\varepsilon \downarrow 0\}$. For our problem, however, the results of this matching procedure are so intuitive that we can dispense with the intermediate steps and simply state the ensuing conditions, which are

$$\begin{aligned} C^{(0)}(0) &= \varpi^{(0)}(\infty), \\ C^{(0)}(0) &= \mu^{(0)}(\infty), \\ \Phi^{(0)}(0) &= \psi^{(0)}(\infty), \end{aligned} \tag{31}$$

as well as

$$\psi^{(0)}_\zeta(\infty) = 0. \tag{32}$$

Let us examine the consequences of these matching conditions. From the expression (27) for the concentration of the positive ions, we have

$$\varpi^{(0)}(\infty) = p_L e^{-\psi^{(0)}(\infty)+V}.$$

On account of the matching conditions (31), the above relation implies that

$$C^{(0)}(0) = p_L e^{-\Phi^{(0)}(0)+V}.$$

Similarly, by considering the concentration of the negative ions, we deduce that

$$C^{(0)}(0) = n_L e^{\Phi^{(0)}(0)-V}.$$

Therefore, by looking at the product and ratio of these two relations we see that

$$\left(C^{(0)}(0)\right)^2 \equiv \frac{1}{4}(J^{(0)})^2\,(a^{(0)})^2 = p_L n_L \tag{33}$$

and

$$\Phi^{(0)}(0) \equiv -\frac{I^{(0)}}{J^{(0)}} \ln a^{(0)} + b^{(0)} = \frac{1}{2} \ln \frac{p_L}{n_L} + V. \tag{34}$$

Thus, we have obtained two relations between the constants $I^{(0)}, J^{(0)}, a^{(0)}$, and $b^{(0)}$. We shall get two additional relations from a consideration of the right boundary layer and thus determine completely the interior solution.

In order to consider the right layer boundary problem, we introduce the appropriate stretched variable

$$\eta = \frac{-1 + x}{\varepsilon} \tag{35}$$

and write the various fields as

$$\begin{aligned} p(1 + \varepsilon\eta; \varepsilon) &= \tilde{\varpi}\ (\eta, \varepsilon), \\ n(1 + \varepsilon\eta; \varepsilon) &= \tilde{\mu}(\eta; \varepsilon), \\ \phi(1 + \varepsilon\eta; \varepsilon) &= \tilde{\psi}(\eta; \varepsilon). \end{aligned} \tag{36}$$

We follow a procedure similar to the earlier one for the left boundary layer; namely, we consider the limit expansions obtained by holding η fixed and letting $\varepsilon \downarrow 0$. Omitting various steps, we simply state that the concentrations are given by

$$\tilde{\varpi} = p_R e^{-\tilde{\psi}^{(0)}(\eta)}, \tag{37}$$

$$\tilde{\mu} = n_R e^{\tilde{\psi}^{(0)}(\eta)}. \tag{38}$$

By means of matching considerations, we then get

$$\left(C^{(0)}(1)\right)^2 \equiv \frac{1}{4}(J^{(0)}(1))^2\left(1 + a^{(0)}\right)^2 = p_R n_R, \tag{39}$$

$$\Phi^{(0)}(1) \equiv -\frac{I^{(0)}}{J^{(0)}} \ln\left(1 + a^{(0)}\right) + b^{(0)} = \frac{1}{2} \ln\left(\frac{p_R}{n_R}\right). \tag{40}$$

As a result, from (34) and (40), we have

$$e^{\Phi^{(0)}(1) - \Phi^{(0)}(0)} = \sqrt{\frac{p_R n_L}{n_R p_L}} e^{-V}. \tag{41}$$

It is easily seen that the product $J^{(0)} a^{(0)}$ is nonnegative. Therefore, if we assume that $J^{(0)}$ and $a^{(0)}$ are positive, we deduce that

$$J^{(0)} = 2\{(p_R n_R)^{1/2} - (p_L n_L)^{1/2}\}. \tag{42}$$

From the expressions for $\Phi^{(0)}(1)$ and $\Phi^{(0)}(0)$, we see that

$$\ln\left(\frac{p_R n_L}{n_R p_L}\right) = -2\frac{I^{(0)}}{J^{(0)}} \ln\left(\frac{1 + a^{(0)}}{a^{(0)}}\right) + 2V. \tag{43}$$

Also, from (33) and (39), we have

$$\frac{1 + a^{(0)}}{a^{(0)}} = \sqrt{\frac{p_R n_R}{p_L n_L}}.$$

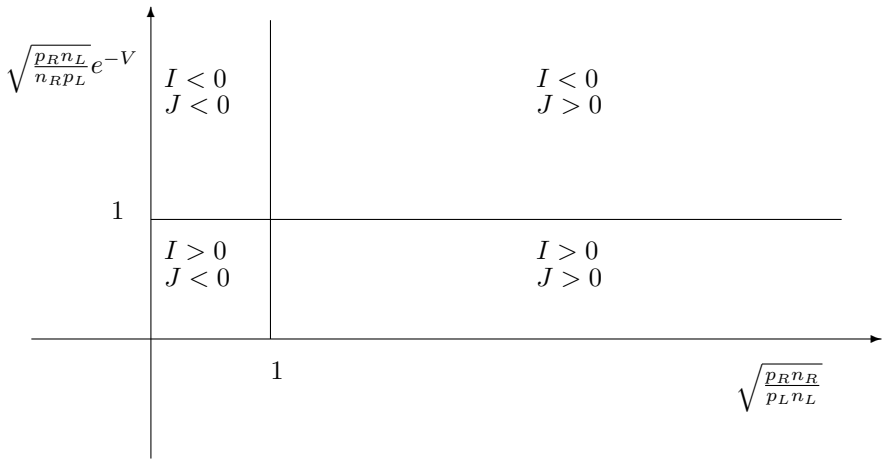

FIG. 1. *The relations between the signs of $I = I^{(0)}$, $J = J^{(0)}$ and the parameters.*

Therefore (see Fig. 1 for sign information),

$$-I^{(0)} = \frac{\ln\left(\frac{p_R n_L}{n_R p_L}\right) - 2V}{\ln\left(\frac{p_R n_R}{p_L n_L}\right)} J^{(0)}. \tag{44}$$

Thus, for p_L, n_L, n_R, p_R fixed, $I^{(0)}$ is a linear function of V, and the sign of $I^{(0)}$ is related to the sign of $\Phi^{(0)}(0) - \Phi^{(0)}(1)$. In summary, the interior fields are completely determined and can be written as

$$C^{(0)} = \sqrt{p_L n_L}(1 - x) + \sqrt{p_R n_R}\, x, \tag{45}$$

$$\Phi^{(0)}(x) = \Phi^{(0)}(0)(1 - F(x)) + \Phi^{(0)}(1)F(x), \tag{46}$$

where

$$F(x) = \frac{\ln\left\{1 - x + \left(\frac{p_R n_R}{p_L n_L}\right)^{1/2} x\right\}}{\ln\left(\frac{p_R n_R}{p_L n_L}\right)^{1/2}}. \tag{47}$$

We now return to the boundary layer version of the Poisson equation at the left end or, more accurately, its integrated form (30). The matching condition (32), together with the fact that $\psi^{(0)}(\infty) = 2^{-1}\ln(p_L/n_L) + V$, implies that

$$c^{(0)^2} = 2(\sqrt{p_L} - \sqrt{n_L})^2. \tag{48}$$

Therefore, if we introduce the new variable

$$s = e^{(\psi^{(0)}(\zeta) - V)/2}, \tag{49}$$

then (30) becomes

$$s' = \pm\frac{1}{\sqrt{2}}\left({n_L}^{1/2} s^2 - {p_L}^{1/2}\right). \tag{50}$$

For ease of writing, we also define

$$a = \left(\frac{p_L}{n_L}\right)^{1/4}$$

and rewrite the previous equation as

$$\frac{s'}{a}\left(\frac{1}{s-a} - \frac{1}{s+a}\right) = \pm\sqrt{2n_L}. \tag{51}$$

An investigation of the consequences of choosing the + sign shows that this sign is inadmissible. Integrating both sides of (51) with respect to ζ, we see that

$$s = \frac{a(1+t)}{1-t}, \tag{52}$$

where

$$t = \left(\frac{1-a}{1+a}\right) e^{\pm\sqrt{2n_L}a\zeta}. \tag{53}$$

Thus, depending on the boundary conditions, one of the following three cases must hold.

(1) If $n_L = p_L$, then $\psi^{(0)}(\zeta) \equiv V$.

(2) If $n_L < p_L$, then

$$\psi^0(\zeta) = V + 2\ln\left(\frac{a(1+\frac{1-a}{1+a}e^{-a\sqrt{2n_L}\zeta})}{1-\frac{1-a}{1+a}e^{-a\sqrt{2n_L}\zeta}}\right), \tag{54}$$

which is an increasing function of ζ on $[0,\infty)$ and is such that $V \le \psi^{(0)}(\zeta) \le V + 2\ln a$.

(3) If $n_L > p_L$, the solution given by (54) is a decreasing function of ζ, with $V + 2\ln a \ge \psi^{(0)}(\zeta) \ge V$.

Using (27), (28), and (54), we now have the following explicit formulas for $\varpi^{(0)}(\zeta)$, $\mu^{(0)}(\zeta)$ on $[0,\infty)$:

$$\varpi(\zeta) = \sqrt{p_L n_L}\left(\frac{1-\frac{1-a}{1+a}e^{-a\sqrt{2n_L}\zeta}}{1+\frac{1-a}{1+a}e^{-a\sqrt{2n_L}\zeta}}\right)^2. \tag{55}$$

$$\mu(\zeta) = \sqrt{p_L n_L}\left(\frac{1+\frac{1-a}{1+a}e^{-a\sqrt{2n_L}\zeta}}{1-\frac{1-a}{1+a}e^{-a\sqrt{2n_L}\zeta}}\right)^2. \tag{56}$$

Similar results hold for $\tilde{\psi}^{(0)}(\eta)$, viz.,

(1) If $n_R = p_R$, $\tilde{\psi}^{(0)}(\eta) \equiv 0$ on $(-\infty, 0)$.

(2) If $n_R < p_R$, then

$$\tilde{\psi}^0(\eta) = 2\ln\left(\frac{a(1+\frac{1-a}{1+a}e^{a\sqrt{2n_R}\eta})}{1-\frac{1-a}{1+a}e^{a\sqrt{2n_R}\eta}}\right), \tag{57}$$

which is a decreasing function of η in the interval $(-\infty, 0]$.

(3) If $n_R > p_R$, then the solution given by (57) is increasing on $(-\infty, 0]$.

Using (37), (38), and (57), we have the following expressions for $\tilde{\varpi}^{(0)}(\eta)$, $\tilde{\mu}^{(0)}(\eta)$ on $(-\infty, 0]$:

$$\tilde{\varpi}^0(\eta) = \sqrt{p_R n_R}\left(\frac{1-\frac{1-a}{1+a}e^{a\sqrt{2n_R}\eta}}{1+\frac{1-a}{1+a}e^{a\sqrt{2n_R}\eta}}\right)^2. \tag{58}$$

$$\tilde{\mu}^0(\eta) = \sqrt{p_R n_R}\left(\frac{1+\frac{1-a}{1+a}e^{a\sqrt{2n_R}\eta}}{1-\frac{1-a}{1+a}e^{a\sqrt{2n_R}\eta}}\right)^2. \tag{59}$$

1.3. Uniformly valid approximations. As is usual with the method of matched asymptotic expansions (cf. [8]), uniformly valid approximations are obtained by first adding the boundary layer solutions to the interior solutions and then subtracting the common parts. Carrying out this simple program, we see that the uniformly valid approximation to the various fields is given as follows.

THEOREM 1.1. *We have the following on* $[0, 1]$*:*

$$\phi(x) = \psi^{(0)}(\varepsilon^{-1}x) + \Phi^{(0)}(x) + \tilde{\psi^0}(\varepsilon^{-1}(1-x)) - \frac{1}{2}\ln\frac{p_R p_L}{n_R n_L} - V + O(\varepsilon), \tag{60}$$

$$\begin{aligned} n(x) &= n_L e^{[\psi^{(0)}(\varepsilon^{-1}x)-V]} + C^{(0)}(x) \\ &\quad + n_R e^{[\tilde{\psi}^{(0)}(\varepsilon^{-1}(x-1))]} - (p_L n_L)^{1/2} - (p_R n_R)^{1/2} + O(\varepsilon), \end{aligned} \tag{61}$$

$$\begin{aligned} p(x) &= p_L e^{[-\psi^{(0)}(\varepsilon^{-1}x)+V]} + C^{(0)}(x) \\ &\quad + p_R e^{[-\tilde{\psi}^{(0)}(\varepsilon^{-1}(x-1))]} - (p_L n_L)^{1/2} - (p_R n_R)^{1/2} + O(\varepsilon). \end{aligned} \tag{62}$$

Remark. We can use the result of section 5 in [9] concerning the contraction principle on a sufficiently short interval by replacing the boundary layer theory with a contraction mapping theory on boundary layers of width d. By selecting the number d to be equal to $\theta\varepsilon$ for sufficiently small θ, the mapping is a contraction in right and left layers. This can be combined with the interior solution as above.

1.4. Remarks on the paper by Cohen and Cooley. In [3], Cohen and Cooley consider the case of several species with concentrations c_i, but for the restricted case of ions with unit charge; i.e.,

$$Z_i^2 = 1.$$

Thus in their notation the governing equations are

$$-\epsilon^2\phi'' = \sum_i Z_i c_i, \tag{63}$$

$$-J_i = c_i' + Z_i c_i \phi'. \tag{64}$$

The boundary conditions are the general boundary conditions; i.e., charge neutrality has not been assumed. We know that the problem for many ions of the *same* charge is identical to the problem for two ions, viz.,

$$-\epsilon^2\phi'' = p - n, \tag{65}$$

$$J_n = n' - n\phi', \tag{66}$$

$$-J_p = p' + p\phi', \tag{67}$$

where

$$n = \sum_i \frac{1 - Z_i}{2} c_i, \qquad p = \sum_i \frac{1 + Z_i}{2} c_i, \tag{68}$$

$$J_n = -\sum_i \frac{1 - Z_i}{2} J_i, \qquad J_p = \sum_i \frac{1 + Z_i}{2} J_i. \tag{69}$$

The authors of [3] prefer to work with the electric field rather than the potential; this is not advisable, since the boundary conditions are prescribed for ϕ rather than E. In fact, this is the source of one of the inconsistencies in their paper. Be that as it may, we follow the analysis of [3] and write the system as

$$\epsilon^2 E' = p - n, \tag{70}$$

$$(p + n)' - (p - n)E = \alpha, \tag{71}$$

$$(p - n)' - (p + n)E = -G, \tag{72}$$

where

$$\alpha = -J_p + J_n, G = J_p + J_n; \tag{73}$$

i.e., G is the current and α is the negative of the total mass flux. Actually, they eliminate $p - n$ altogether and make use of

$$C' - \epsilon^2 E E' = \alpha, \tag{74}$$

$$\epsilon^2 E'' - CE = -G, \tag{75}$$

where $C = p + n$. Of course, one of these equations can be integrated to yield

$$C = \alpha x + \beta + \frac{\epsilon^2}{2} E^2,$$

where β is a constant of integration. In order to bring out the physical meaning of the various terms, they rewrite this equation as

$$\begin{aligned} C &= \alpha x + (p_L + n_L) + \frac{\epsilon^2}{2}(E^2 - E_0^2) \\ &= \left[p_R + n_R - p_L - n_L - \frac{\epsilon^2}{2}(E_1^2 - E_0^2)\right] x + (p_L + n_L) + \frac{\epsilon^2}{2}(E^2 - E_0^2). \end{aligned} \tag{76}$$

This is the expression which they choose to use in order to eliminate C from the problem. The result is

$$\epsilon^2 E'' - \left\{ \left[p_R + n_R - p_L - n_L - \frac{\epsilon^2}{2}(E_1^2 - E_0^2)\right] x + (p_L + n_L) + \frac{\epsilon^2}{2}(E^2 - E_0^2) \right\} E + G = 0.$$

They then attempt to get an asymptotic solution of this equation for $\epsilon << 1$. In the process of deriving the asymptotic expansion, they make two errors. The first stems from the fact that they do not solve the boundary layer equations. Rather, they "guess" the form of the solution in the boundary layer and substitute this functional form into the equation to determine some of the minor dependencies. The second error stems from the fact that they assume that constants such as E_0, E_1 are $O(1)$. In our approach, we actually solve the boundary layer equations and can check a posteriori

that the form assumed in [3] is not the correct one. We also find in the process that the potential has very steep gradients near the endpoints. This means that the electric fields near the endpoints are very large and that E_0, E_1 are in fact of order $O(\epsilon^{-1})$. The two errors are inextricably tied to each other. Indeed, an incorrect order for E_0, E_1 leads to an incorrect boundary layer equation, into which is substituted an incorrect functional form of the solution.

2. Numerical simulations and discussion. In this section, we shall present simulations for appropriately selected parameter sets, with the following goals:

(i) The illustration of the qualitative features developed in sections 3 and 4 of [9],

(ii) A careful comparison of the (numerical) solution with that calculated by singular perturbation methods. Both the interior solution and the uniformly valid approximation (also called the full solution) are studied for the singular perturbation case.

The PNP systems (equations (1)–(3)), with boundary conditions (equations (4)–(6)), are solved numerically by Gummel's iteration [4]. The details of the discretization are described in [2] and are discussed in the following section. We have used a 30Å-long channel and a relative dielectric constant of 80 in our simulation. It takes only a few seconds to calculate both the numerical solution and the singular perturbation solutions with 3000 equidistant gridpoints on our IBM/RS6000 model 550 workstation.

For such a channel, the value of the parameter ε is 8.7×10^{-2}. Since the square of this parameter is small, the singular perturbation analysis ought to provide good approximations to the various fields as well as to the overall current and flux. However, since the leading asymptotic expressions are independent of various parameters such as $\rho_L = p_L/n_L$ and $\rho_R = p_R/n_R$, the accuracy of expressions is difficult to assess. To that end, we shall systematically compare the approximations derived in section 1 with the numerical simulations of the exact solutions. Recall that in terms of the numbers ρ_L, ρ_R, the primary categories can be described by

$$(\text{BC1}): \ \rho_L \le 1, \quad \rho_R \ge 1, \tag{77}$$

$$(\text{BC2}): \ \rho_L \le 1, \quad \rho_R \le 1, \tag{78}$$

$$(\text{BC3}): \ \rho_L \ge 1, \quad \rho_R \le 1, \tag{79}$$

$$(\text{BC4}): \ \rho_L \ge 1, \quad \rho_R \ge 1. \tag{80}$$

All the figures displaying the concentrations and potential fields also display either the corresponding interior fields, given in (45), (46), or the uniformly valid approximations, given in (60)–(62). Also, we have listed in Table 1 the values of the fluxes and currents obtained by asymptotic techniques, with the corresponding computed numerical values.

The total flux of the singular perturbation interior solution is computed according to (42) and the electric current according to (44). The individual fluxes are computed from the combination of the total flux and electric current. To evaluate the fluxes according to the uniformly valid approximation, we use the potential profile of (60) and the values of $p_L{=}\varpi(0)$, $p_R{=}\tilde{\varpi}(0)$, $n_L{=}\mu(0)$, $n_R{=}\tilde{\mu}(0)$ in the formulas

$$J_n = \frac{n_R e^V - n_L}{\int_0^1 e^{\phi_0 - \phi(x)} dx}, \tag{81}$$

$$J_p = -\frac{p_R e^{-V} - p_L}{\int_0^1 e^{-\phi_0 + \phi(x)} dx} \tag{82}$$

TABLE 1
Parameters used in the numerical simulations.

p_L	n_L	p_R	n_R	V	J_p J_p^{SPIS} J_p^{SPFS}	J_n J_n^{SPIS} J_n^{SPFS}	J J^{SPIS} J^{SPFS}	I I^{SPIS} I^{SPFS}	ϵ
1	1	4	4	2	1.29 1.32 1.32	7.45 7.33 7.33	6.16 6.00 6.00	8.74 8.66 8.66	8.72×10^{-2}
1	1	4	4	8	1.22×10^{1} 1.43×10^{1} 1.43×10^{1}	2.05×10^{1} 2.03×10^{1} 2.03×10^{1}	8.27 6.00 6.00	3.27×10^{1} 3.46×10^{1} 3.46×10^{1}	8.72×10^{-2}
1	3	4	2	1	-8.21×10^{-1} -8.64×10^{-1} -8.31×10^{-1}	1.36 1.33 1.35	2.19 2.19 2.18	5.43×10^{-1} 4.66×10^{-1} 5.17×10^{-1}	8.72×10^{-2}
0.1	30	4	2	1	-5.22 -6.01 -5.31	-5.53 -3.82 -5.30	-3.05×10^{-1} 2.19 1.41×10^{-2}	-1.08×10^{1} -9.83 -1.06×10^{1}	8.72×10^{-2}
10	0.3	4	2	1	8.11 7.68 8.13	2.23 2.28 2.23	-5.88 -5.30 -5.90	1.04×10^{1} 1.01×10^{1} 1.04×10^{1}	8.72×10^{-2}
1	6	6	9	1	-3.10 -3.53 -3.18	6.82 6.27 6.66	9.93 9.80 9.84	3.73 2.74 3.49	5.81×10^{-2}
1	6	6	9	4	1.04×10^{1} 1.43×10^{1} 1.05×10^{1}	2.35×10^{1} 2.41×10^{1} 2.49×10^{1}	1.30×10^{1} 9.80 1.44×10^{1}	3.39×10^{1} 3.84×10^{1} 3.54×10^{1}	5.81×10^{-2}
4	1	1	9	4	1.72×10^{1} 1.33×10^{1} 1.66×10^{1}	2.04×10^{1} 1.53×10^{1} 1.95×10^{1}	3.16 2.00 2.91	3.16×10^{1} 2.86×10^{1} 3.62×10^{1}	5.81×10^{-2}

Note: SPIS denotes the singular perturbation interior solution, and SPFS denotes the singular perturbation full solution.

as the values of the approximated boundary conditions. Those values are the values of the uniformly valid approximation for concentrations evaluated at the two boundaries.

In Fig. 2, we show the concentration profiles and the electric potential profile for the case of simple boundary conditions (Case 1). The curves show the basic features summarized in section 3.3 of [9], and they are $\phi_x < 0$, $\phi_{xx} \geq 0$, $n \geq p$, $n_x, p_x \geq 0$. The fact that $IV, J \geq 0$ is supported in Table 1. Note the agreement with Theorems 3.1 and 3.2. The singular perturbation interior solution and the uniformly valid approximation are identical for simple boundary conditions; therefore, they give the same fluxes and electric current in Table 1. In Fig. 2(a), the electric potential is monotonic decreasing and is concave upward. In Fig. 2(b), the singular perturbation solution gives $p(x) = n(x)$, and these identical curves are intermediate between the calculated $p(x)$ and $n(x)$ of the solution for the case $V = 2$. However, it gives a less accurate solution when V is increased to $V = 8$, as expected, because the singular perturbation solution is independent of V.

Figure 3 compares the numerical solution with the singular perturbation *interior* solution for both BC1 and BC4, as developed in section 4 of [9]. Figure 3(a) shows the electrical potential profiles. The solid lines indicate the numerical solutions, and the dashed lines the singular perturbation interior solutions. On the same graph, we show the comparison of three choices of boundary conditions which have the same product

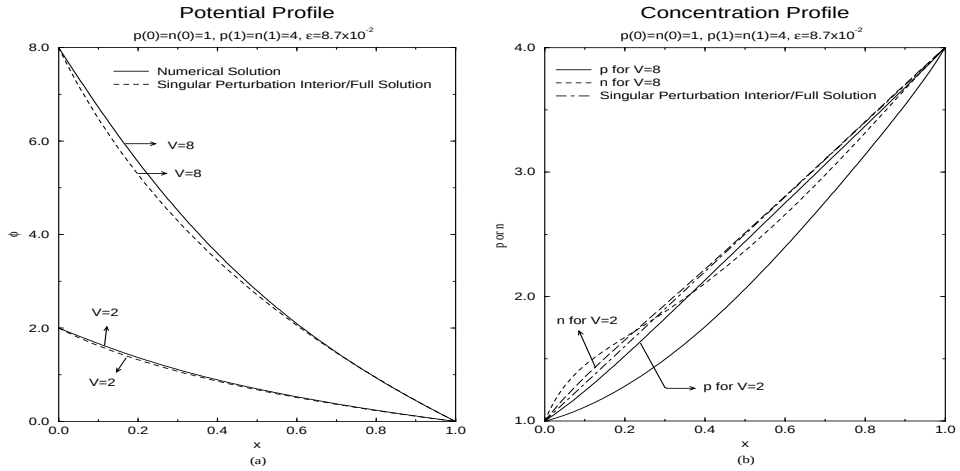

FIG. 2. *The electric potential profile and concentration profiles for the simple boundary condition, Case* 1. *Dimensionless concentration and potential units employed. Original units of* 100 *mM and* 25 *mV, resp.*

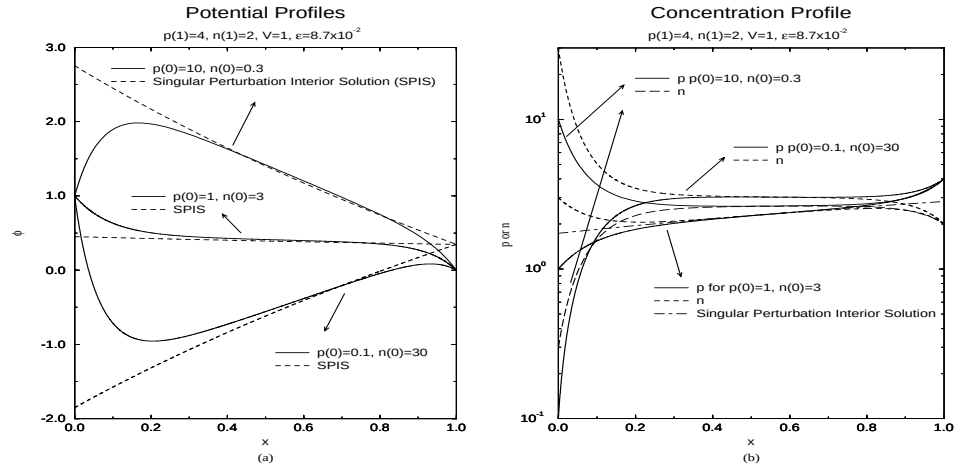

FIG. 3. *The comparison of the numerical solution and the singular perturbation interior solution for the general boundary conditions* BC1 *and* BC4.

$p(0)n(0)$. Figure 3(a) shows the remarkable confirmation of Lemma 4.4, in that when $I \geq 0$ (the case $p(0) = 1, n(0) = 3$), then the electric potential is a decreasing function; however, the other instance of BC1 in that figure ($p(0) = .1, n(0) = 30$) leads to a negative current and a nonmonotone potential. Figure 3(a) also clearly shows that even though the singular perturbation interior solution is a reasonable approximation for the case $p(0) = 1$, $n(0) = 3$ of BC1, it is not a good approximation for other choices of BC1 or for BC4 when $p(0)$ and $n(0)$ are very different. The concentration profiles show more contrast in Fig. 3(b). The singular perturbation interior solution (SPIS) gives the *same* profile for all three choice of parameters. In the SPIS, $p(x) = n(x)$, shown by the dot-dashed line, which falls between the profile of the numerical solution of p and n *only* when $p(0) = 1$, $n(0) = 3$. But the SPIS does not at all approximate the other two numerical solution profiles of BC1 and BC4. The numerical solutions

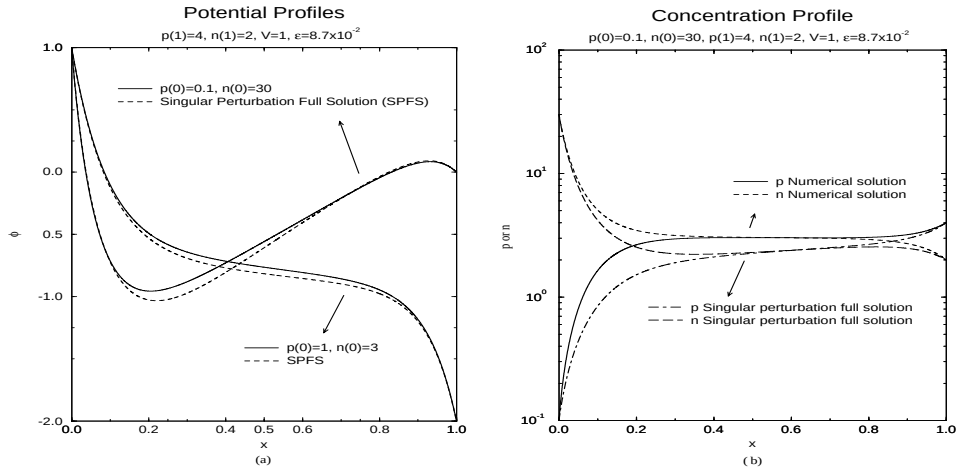

FIG. 4. *The comparison of the numerical solution and the singular perturbation full solution for the general boundary condition* BC1.

consistently satisfy Proposition 4.3. Thus, we see the crossing pattern predicted by that result. Also, a version of Theorem 4.6 for BC4 holds; $IJ \leq 0$ and the curve for p dominates that for n.

Although the singular perturbation *interior* solution does not yield good quantitative results for the parameter choice of $p(0) = .1$, $n(0) = 30$ of BC1, the singular perturbation *full* solution still gives a very accurate approximation. We show this in Fig. 4. In Fig. 4(a), we show the comparison of the electric potential profiles of the numerical solution with those from (60) for two choices of BC1, and we show only the concentration profiles for $p(0) = .1$, $n(0) = 30$ in Fig. 4(b), because the interior solution is a good approximation already for $p(0) = 1$, $n(0) = 3$. Figure 3 already has shown the large deviation of the interior solution, (46), from the numerical solution, which is also reflected in the value of the total flux in Table 1. But the curves of the uniformly valid approximation, which incorporates the solution of the boundary layers, can still closely follow the curves from the numerical solution—a great improvement over the interior solution. Our simulations thus show the boundary layers are long range, even when the numerical value of ϵ is small. Despite the improvement in using the full singular perturbation solution, the sign of the total flux differs from the numerical solution because the absolute value of the flux is small in this case, and small errors may cause the total flux to change its sign. For $p(0) = 10$, $n(0) = 0.3$, the uniformly valid approximation improves even more. In this case, it faithfully gives very accurate solutions in all aspects: the profiles, the total flux, and the electric current.

We recall from section 4 of [9] that BC1 and BC2 exhibit very different qualitative behavior. In fact, for BC2, we expect that the curve for n will dominate the curve for p, at least when $IJ \geq 0$, according to Theorem 4.6 of [9]. This is confirmed by the plots of Fig. 5. We also show comparisons of the numerical solution with the singular perturbation solution for BC2. In Fig. 5, we plot the potential profile and concentration profiles for the case of $p(0) = 1, n(0) = 6, p(1) = 6, n(1) = 9, V = 1$. We plot the potential profile of the numerical solution, the profile of the singular perturbation interior solution, and that of the singular perturbation uniformly valid approximation. In Fig. 5(a), the solid line is the numerical solution, the dashed line with triangle symbols is the profile of the singular perturbation interior solution, and the long dashed line with circles is the profile of the singular perturbation uniformly valid approximation. The graph clearly shows how the boundary layers and interior

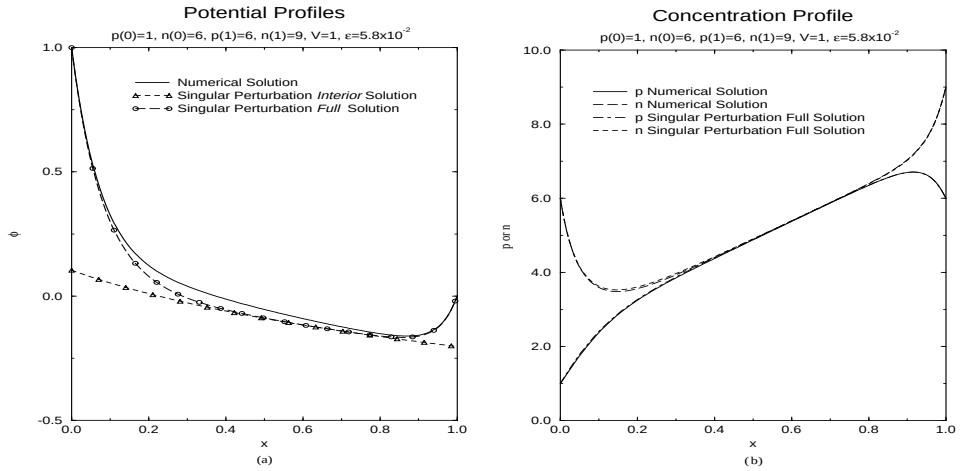

FIG. 5. *The comparison of the numerical solution and the singular perturbation full solution for the general boundary condition* BC2.

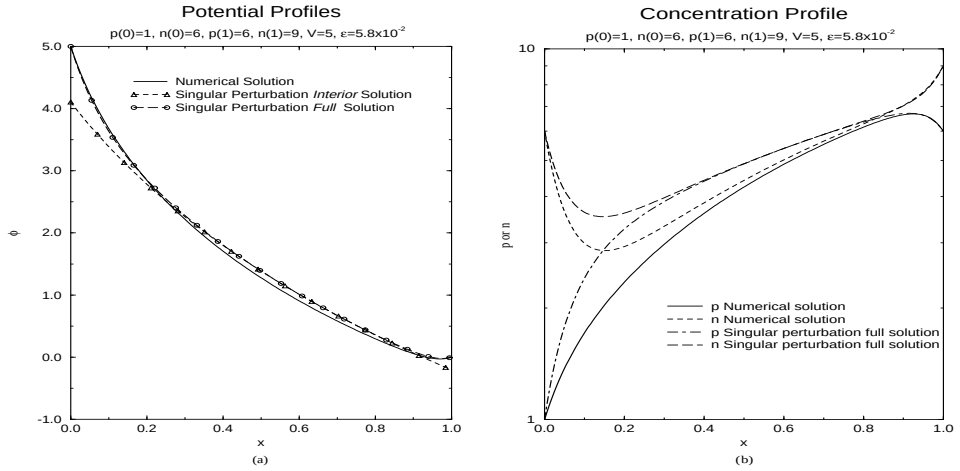

FIG. 6. *The comparison of the numerical solution and the singular perturbation full solution for the general boundary condition* BC2 *with a large* V. *The same convention is used as in Fig.* 5.

solution make up the uniformly valid approximation, which is an accurate approximation for this case. In Fig. 5(b), the solid line and the dashed line are the numerical solution of the p-concentration profile and the n-concentration profile, respectively. The dot-dashed line is the p-concentration profile of the singular perturbation, and the long dashed line is the n-concentration profile of the singular perturbation. The plot of concentration profiles show the singular perturbation uniformly valid approximation and the numerical solution are nearly identical for this case. The comparison of fluxes and the electric current in Table 1 confirms this conclusion.

In Fig. 6, we show the effect of large bias potentials. We keep the same concentration boundary conditions and increase V to 5. We recall from the classification scheme, introduced in section 4.1 of [9], that such crossing of parameter space may reverse the sign of one of the individual flux components, and, indeed, this occurs.

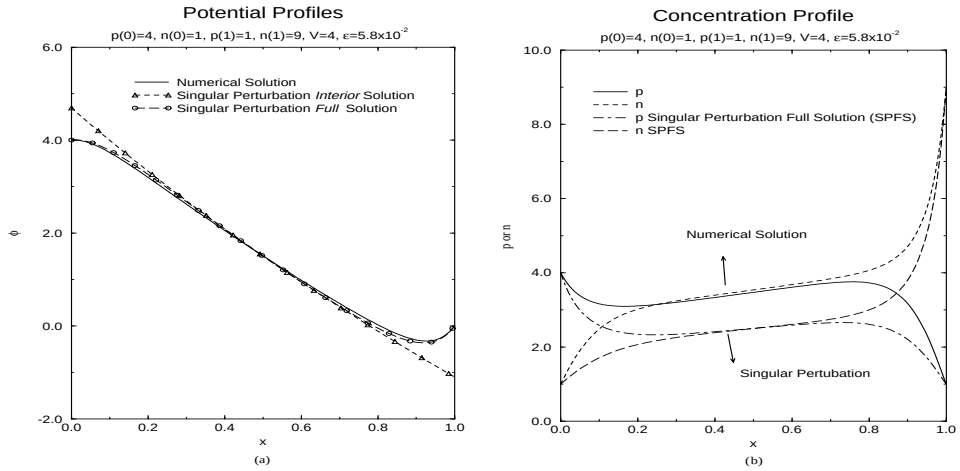

FIG. 7. *The comparison of the numerical solution and the singular perturbation full solution for the general boundary condition* BC3 *with a large* V. *The same convention is used as in Fig.* 5.

According to the characterization, $J_n > 0$, $J_p > 0$, if and only if

$$\max\left(\ln\left(\frac{n_L}{n_R}\right),\ \ln\left(\frac{p_R}{p_L}\right)\right) < V. \tag{83}$$

We now expect both J_n and J_p to be positive, and this is confirmed by Table 1. In this case, even though the electric potential profile of the singular perturbation uniformly valid approximation shown in Fig. 6(a) does not differ much from the numerical solution, the concentration profiles in Fig. 6(b) in fact do. The concentration profiles of the singular perturbation uniformly valid approximation predict a charge neutral central region, whereas the numerical solution gives no charge neutral region at all. We can expect a large deviation in the fluxes and the electric currents from the two calculations, as is shown in Table 1.

We show the comparison of the numerical solution with the singular perturbation solution for BC3 in Fig. 7. The concentration plot shows again that there is a large deviation of the singular perturbation uniformly valid approximation from the numerical solution when V is large. The calculations with the same concentration boundary conditions, but with $V = 1$, show both are nearly identical, as shown in Fig. 5. Recall that BC3 is the mirror image of BC1. This is confirmed by the crossing pattern of the concentration curves, consistent with the mirror image of Proposition 4.3 [9]. The potential profile is not monotone, and this is consistent with the fact that $I > 0$. We would require $I \leq 0$ to conclude that the potential is increasing, as the counterpart to Lemma 4.4 [9]. Thus, the singular perturbation full solution gives an accurate approximation in all the domains we have examined, except for the following two cases: (1) large bias potential V and (2) significantly large values of ρ_L and/or ρ_R.

We shall now present a final summation. The PNP model describes a physically simple system of ions, diffusing and migrating between regions of fixed concentration and potential, ions that move in fields created by their own concentrations as well as the boundary sources. As simple as the system is, it requires rather careful analysis, because different behaviors occur depending on the relative direction of electrical and concentration gradients.

When permanent charge is present, the richness of behavior is considerably increased. Indeed, the PNP equations in a suitably complicated branched one-dimen-

sional domain can describe all the properties of an integrated circuit, thus a microprocessor with memory, thus all the information that can be encoded or processed by a computer! The qualitative properties of semiconductor devices are determined by their one-dimensional distribution of permanent charge; it also seems likely that many of the properties of ionic channels (in biological membranes) are determined this way as well.

Thus, extension of our study to systems of permanent charge is of considerable interest. The work of this paper suggests that each domain of driving forces will need separate analysis. Each class of permanent charge distribution will also probably require separate analysis. The interest of the PNP model with permanent charge is in the richness of behavior it encompasses; it would be unrealistic (and disappointing) to expect that such behavior could be described by universal formulas, valid in all domains less vague than the global conservation of mass, charge, energy, etc.

Universal formulas describing quantitative properties in *some* domains (i.e., those of engineering or biological importance) should not be shunned because of their limited domains of validity. Semiconductors and channels change their qualitative properties as boundary conditions are changed, and so analysis of the qualitative properties of each domain would be of great use, and some beauty.

3. The discretization. We have taken advantage of the fact that the one-dimensional Nernst–Planck equation (the drift–diffusion equation) can be integrated analytically to yield a formula for the concentration of carriers of valence z for $x \in [L, R]$:

$$c(x) = \frac{1}{\int_L^R e^{z\phi(\zeta)d\zeta}} \left[c_L e^{z(\phi_L - \phi(x))} \int_x^R e^{z\phi(\zeta)} d\zeta + c_R e^{z(\phi_R - \phi(x))} \int_L^x e^{z\phi(\zeta)} d\zeta \right]. \tag{84}$$

c stands for p and n when $z = 1$ and $z = -1$, respectively. If we make a linear approximation of the potential profile, letting

$$\phi(x) = \phi_L + \frac{(\phi_L - \phi_R)}{(x_R - x_L)} x \quad \text{for } x \in [L, R]\,, \tag{85}$$

the carrier concentration is then well defined.

Therefore, if the following basis function is chosen between mesh points, in the sense of a generalized spline,

$$\eta_i = \frac{1}{(x_{i+1} - x_i)} \left[1 - \left| \frac{x - x_i}{x_{i+1} - x_i} \right| \right], \tag{86}$$

we then can discretize the Poisson equation by expanding the function with this basis set on the mesh. To obtain the expansion coefficient, we multiply the Poisson equation by the function η_i and integrate over $[x_{i-1}, x_{i+1}]$. We get, for a uniform mesh,

$$\begin{aligned} & \varepsilon^2(\phi_{i+1}^{(m+1)} - 2\phi_i^{(m+1)} + \phi_{i-1}^{(m+1)}) \\ = & \left(\sum_k z_k^2 c_k^{(m,i)} \right) (\phi_i^{(m+1)} - \phi_i^{(m)}) - \sum_k z_k c_k^{(m,i)} \\ & - \sum_k z_k (c_k^{(m,i+1)} - c_k^{(m,i)}) f[z_k(\phi_i^{(m)} - \phi_{i+1}^{(m)})] \\ & + \sum_k z_k (c_k^{(m,i)} - c_k^{(m,i-1)}) f[z_k(\phi_i^{(m)} - \phi_{i-1}^{(m)})]\,, \end{aligned} \tag{87}$$

where

$$f(\tau) \equiv \begin{cases} \frac{1}{6} & \text{for } \tau = 0 \ , \\ \frac{e^{\tau}-1-\tau-\frac{1}{2}\tau^2}{\tau^2(e^{\tau}-1)} & \text{for } \tau \neq 0 \ . \end{cases} \tag{88}$$

m denotes iteration index, i is the mesh point index, and z_k is the valence of the kth carrier species.

There is no need to discretize the drift–diffusion equation; the concentration can be updated by (84) for each iteration. To ensure the continuity of flux, the flux will be evaluated according to the analytic expression over the entire domain

$$J_k = \frac{D_k}{\int_0^1 e^{z_k \phi(\zeta)} d\zeta} (c_k(0) e^{\phi(0)} - c_k(1) e^{\phi(1)}) \ . \tag{89}$$

The experimental measured quantity—electrical current—is then evaluated by $I = \pi a^2 \sum_k z_k J_k$.

The convergence of this iteration has been studied in depth in the literature. For this model, no difficulties were observed. However, the interpretation of the underlying mapping as a contraction has proven fruitful (see [9]). A very revealing study, showing that for certain parameter ranges the iteration can approach the solution and then diverge, has been carried out in [7]. For the reader interested in the underlying methodology, one is actually employing a global exponential fit to the continuity subsystem, and a piecewise linear fit to the Poisson equation, linked to a system decoupling fixed point iteration (Gummel iteration).

REFERENCES

[1] V. Barcilon, D.-P. Chen, and R.S. Eisenberg, *Ion flow through narrow membrane channels: part* II, SIAM J. Appl. Math., 52 (1992), pp. 1405–1425.

[2] D.-P. Chen and R.S. Eisenberg, *Charges, currents, and potentials in ionic channels of one conformation*, Biophys. J., 64 (1993), pp. 1405–1421.

[3] H. Cohen and J. Cooley, *The numerical solution of the time dependent N-P equation*, Biophys. J., 5 (1965), pp. 145–162.

[4] H.K. Gummel, *A self-consistent iterative scheme for one-dimensional steady state transistor calculations*. IEEE Trans. Electron Devices, ED-11 (1964), pp. 455–465.

[5] B. Hille, *Ionic Channels of Excitable Membranes*, 2nd ed., Sinauer Associates, Sunderland, MA, 1992.

[6] J.W. Jerome, *Analysis of Charge Transport: A Mathematical Study of Semiconductor Devices*, Springer-Verlag, Berlin, 1996.

[7] T. Kerkhoven, *On the effectiveness of Gummel's method*, SIAM J. Sci. Statist. Comp., 9 (1988), pp. 48–60.

[8] J. Kevorkian and J. Cole, *Perturbation Methods in Applied Mathematics*, Springer-Verlag, New York, 1981.

[9] J.-H. Park and J.W. Jerome, *Qualitative properties of steady-state Poisson-Nernst-Planck systems: Mathematical study*, SIAM J. Appl. Math., 57 (1997), pp. 609–630.

[10] I. Rubinstein, *Electro-Diffusion of Ions*, SIAM Studies in Applied Mathematics, SIAM, Philadelphia, PA, 1990.